Advanced Intelligent Systems

ADVANCED INTELLIGENT SYSTEMS Open Access

www.advintellsyst.com

RESEARCH ARTICLE OPEN ACCESS

OriGrasp: A Multifunctional Origami-Inspired Instrument for Delicate Manipulation in Abdominal Surgery

Lorenzo Mocellin | Niccolò Pagliarani | Giulia Gamberini | Gastone Ciuti | Matteo Cianchetti | Arianna Menciassi

The BioRobotics Institute, Sant'Anna School of Advanced Studies, Pisa, PI, Italy

Correspondence: Lorenzo Mocellin (lorenzo.mocellin@santannapisa.it)

Received: 6 October 2025 | **Revised:** 30 December 2025 | **Accepted:** 9 January 2026

Keywords: reconfigurable instrument | origami design | compliant mechanism | robotic surgery | delicate tissue manipulation

ABSTRACT

Conventional instruments for minimally invasive surgery (MIS) face challenges in terms of miniaturization and compliance with soft tissues due to their tiny yet rigid structure. In abdominal surgery, rigid instruments increase the risk of bowel injury, as this tissue is extremely delicate and prone to peeling, stretching, or tearing. By leveraging the principles of origami, instruments can be designed and fabricated by folding 2D shapes, simplifying the manufacturing process. The foldability enables the creation of reconfigurable instruments capable of performing multiple functions, all while operating through tiny access ports and within narrow cavities with minimal invasiveness. This paper presents a deployable origami-inspired instrument for robot-assisted MIS, characterized by lightweight construction and tunable compliance. The foldable design supports multiple surgical functions, enabling the integration of additional tools at the tip in its unfolded configuration or functioning as a grasper for tissue manipulation once deployed. In grasper mode, the flexible structure is designed to deform upon contact with surrounding tissues, either during insertion into narrow cavities or when the grasper is actuated. This deformation ensures a secure and safe grasp of the tissues. The maximum pinch force achieved by the grasper is 4 N, while the pulling and lifting forces are within the range reported in literature for atraumatic manipulation of bowel tissue (0.18–1.21 N). The grasper's jaws were studied in terms of material selection and geometry to achieve a compromise between soft grasping and effective pulling force. Experimental tests demonstrated the grasper's capability not to apply excessive pressure on the tissue (well below the safety threshold of 329 kPa for bowel tissue), while maintaining a firm grasp during the manipulation of ex vivo porcine bowel tissue. Finally, the successful integration of the instrument into a da Vinci Research Kit robotic platform highlights its potential usability in surgical scenarios.

1 | Introduction

Minimally invasive surgery (MIS) has transformed clinical practice by reducing patient trauma, postoperative pain, and hospitalization time [1]. Robotic-assisted platforms, such as the da Vinci Surgical System (Intuitive Inc., USA), have further enhanced MIS by enabling high precision, motion scaling, and improved dexterity in confined anatomical environments [2, 3]. However, designing dexterous instruments for MIS remains challenging, as they must be miniaturized to pass through small ports and manipulate delicate tissues [4]. These requirements lead to mechanically complex architectures composed of numerous tiny rigid components, such as brackets, pins, joints, and bolts [5, 6], which increase production costs and raise hygiene concerns due to residue-retaining gaps and complex sterilization protocols [7]. Moreover, their rigid architecture limits compliance with soft tissues, thus increasing the risk of stress concentration and iatrogenic damage [8]. These issues are particularly critical in abdominal procedures, such as bowel handling [9], where the bowel's high sensitivity to compressive stress makes it vulnerable to bleeding, inflammation, ischemia, and postoperative complications like adhesions or obstructions [10–13]. The challenges and limitations of current solutions highlight the need for compliant, miniaturized and inherently safe robotic instruments that are also cost-effective and durable despite wear and

sterilization requirements. In this context, origami-inspired designs offer a promising alternative, since they are inherently modular, deployable and easy to fabricate, making them an attractive approach for medical devices delivered through minimally invasive access ports [14, 15]. Previous studies have demonstrated the potential of using origami in designing tiny and compact surgical instruments, such as the foldable surgical forceps presented in [16], the 4-DoF origami grasper in [17], the mini-RCM (an origami-inspired manipulator for eye surgery) [18], or the battery-free micro-origami arm shown in [19]. However, most of these efforts concentrated on miniaturization or structural simplification, leaving unexplored the use of pure origami designs for instruments tailored to delicate tissue manipulation in abdominal surgery.

Conversely, instruments specifically designed for handling delicate tissues, such as [20], prioritize maximizing contact area and often incorporate force sensors. However, they retain a rigid structural design, which limits their ability to conform to soft anatomical surfaces. Other approaches, such as the one proposed by Kinnikut et al. [8], combine soft actuators with embedded sensors to improve compliance and enable safer tissue interaction. While promising, the grasper presented in [8] is primarily intended for static tasks such as bowel retraction rather than for continuous and dynamic manipulation. Furthermore, its relatively bulky form factor, requiring an 18 mm trocar, limits its suitability for traditional MIS. An alternative strategy for atraumatic tissue handling is represented by suction-based devices, such as the one described in [21]. While these solutions avoid rigid mechanical contacts, they still face limitations in terms of miniaturization and adaptability to the constrained and variable anatomy encountered in MIS procedures.

To address these limitations, specifically the trade-off between compliance and compactness, we introduce OriGrasp, a novel robotic instrument designed for safe manipulation of bowel tissue. OriGrasp leverages origami-inspired principles to simplify structure and fabrication while preserving functionality in a compact form suitable for MIS. The origami-inspired design enables OriGrasp to flatten, facilitating both compact storage and sterilization. In particular, unlike many current instruments with sophisticated assemblies that are difficult to sterilize, the flat configuration fully exposes all components, allowing for faster and more effective cleaning.

The foldable structure enables insertion through standard 12 mm trocars and compliant interaction with delicate tissues in constrained anatomical cavities. A key feature distinguishing OriGrasp from previously reported origami-inspired devices is its reconfigurable design, which allows switching between two roles: (i) an introducer for interchangeable tools (e.g., suction-irrigation units, sensorized probes, or sampling catheters) and (ii) a compliant grasper for delicate tissue manipulation. Reconfigurability is achieved using the same actuation system that drives the grasper, avoiding additional actuators and reducing system complexity. The combined introducer function can streamline instrument deployment and reduce tool exchanges during surgery. When configured as a grasper, the instrument passively modulates the applied forces through its deformable structure, acting as a mechanical fuse that redirects excessive forces through the flexible joints. This self-limiting behavior allows intrinsic regulation of grasping forces without added electronics, resulting in a device that is easier to manufacture, maintain, and sterilize. Furthermore, unlike several comparable devices reported in the literature, which were not evaluated on a commercial surgical robotic platform, OriGrasp is validated in a standard MIS workflow through its integration with the da Vinci Research Kit (dVRK) platform. This aspect is highlighted in the comparative analysis presented in Section 4.4.

In this work, OriGrasp was characterized in terms of grasping performance, specifically examining the trade-off between pinch force and safe tissue handling of soft tissues. The maximum pinch force reached by the grasper was 4 N, with an actuation force of 10 N, resulting in a transmission efficiency of 40%. The measured pulling and lifting forces on bowel tissue ranged between 0.6 and 0.9 N. These results are consistent with values reported in literature for safe bowel tissue handling, confirming the potential of OriGrasp in minimally invasive abdominal procedures.

Finally, the integration with a da Vinci surgical system demonstrated the feasibility of its seamless adoption in robotic surgery.

2 | OriGrasp: A Rigidly Foldable Origami Surgical Instrument

OriGrasp is a robotic surgical instrument (Figure 1A) devised to achieve a simplified, miniature and lightweight design. It exploits the origami concept, in which complex 3D shapes are formed by folding flat sheets, to enable compactness and deployable functionality. Developed within the framework of thick rigidly foldable origami mechanisms, as defined by Lang et al. [22], OriGrasp relies on stiff sheet-like panels connected by thin flexible hinges. Unlike traditional origami, where sheets may bend and stretch during folding, rigid origami confines motion to the hinges while keeping undeformable panels [22, 23]. This principle allows OriGrasp to transition smoothly between configurations, for example, from the unfolded state to the grasper mode, in a predictable way and without structural distortion. As a result, the device achieves precise motion and mechanical robustness, making it suitable for surgical tasks. Moreover, while many origami-inspired mechanisms emphasize compact storage and deployment but remain static once unfolded, OriGrasp instead belongs to the class of action origami systems. These mechanisms, as described in [24], retain mobility in their deployed state and are capable of repeated motion. In the case of OriGrasp, this translates into a device that can grasp and release objects dynamically, extending the origami paradigm beyond static deployability.

OriGrasp is miniaturized to integrate onto a 10 mm shaft, making it suitable for insertion through access ports commonly used in abdominal minimally invasive procedures [25]. Its foldable design enables the instrument to collapse and be stored within the shaft using two dedicated housings (Figure 1B). In the unfolded state, the central channel remains unobstructed, allowing additional surgical tools to pass through the same shaft and reach the operative site without interference.

The jaws of the grasper were designed with a length of 10 mm, typical of conventional graspers [26], and a width of 5 mm, yielding a 50 mm^2 contact area. Its foldable structure allows a versatile opening angle, reaching 60 deg in the interlocked configuration to 180 deg when fully detached (Figure 2B). Moreover, unlike conventional laparoscopic graspers with fixed V-shaped jaws, OriGrasp allows for free reorientation of the jaws upon tissue

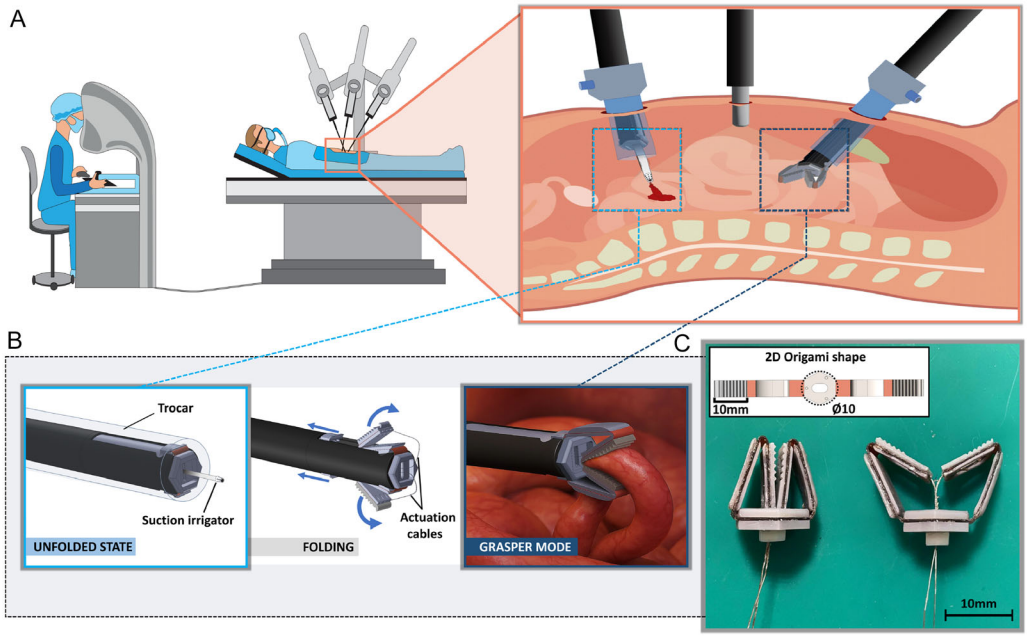

FIGURE 1 | Illustration of OriGrasp. The instrument is used in robotic surgery to target the abdominal cavity (A). The instrument, shown in (B), can switch from an unfolded state, where it is used as an introducer for another instrument (e.g., suction irrigator), to the grasper mode, tailored for delicate tissue manipulation, e.g., bowel tissue. The origami-inspired design shown in (C) helps in easy prototyping and miniaturization. The current prototype features a 10 mm diameter and 10 mm jaws.

contact, enabling parallel alignment with the surface for secure grasping, thereby closely replicating clinically validated bowel graspers [27]. Heijnsdijk et al. [28] reported 3.3 N as the minimum force required to prevent slippage during tissue grasping. Accordingly, we targeted a 4 N pinch force to provide a safety margin for stable grasping during common MIS maneuvers (e.g., retraction, exposure, and tissue positioning). However, grasping safety does not depend on pinch force alone. The pressure transmitted to the tissue varies with the geometry of the jaws, in particular the presence and spacing of teeth, and the effective contact area, meaning that the same applied pinch force can result in different local pressures. Defining a pressure threshold is clinically important, since the bowel is highly sensitive to localized compressive stress. Such pressure can lead to intestinal adhesions and complications, including obstruction, chronic pain, infertility, and perforation, thereby increasing postoperative morbidity and mortality [29]. For this reason, a conservative compressive pressure threshold of 329 kPa was adopted from Khan et al. [29], which quantified bowel and colon tolerance under localized compression using a 19.6 mm^2 circular indenter. By combining both force- and pressure-based limits, these thresholds were selected to ensure that OriGrasp handles bowel tissue atraumatically during robotic minimally invasive procedures, reducing the risk of excessive loading. Pulling and lifting forces were interpreted against Ranzani et al. [12], which reports ranges representative of gentle tissue manipulation commonly performed in clinical practice (e.g., atraumatic traction and lifting for exposure). The desired efficiency, defined as the ratio of grasping to actuation force, was established at 0.4, consistent with commercial atraumatic graspers [30]. The specifications of the device are summarized in Table 1.

While force and pressure thresholds provide guidelines, tissue damage also depends on duration and frequency of loading. To minimize risks, OriGrasp is featured by a compliant structure that reduces peak pressures, distributes forces uniformly and acts as a mechanical fuse: flexible joints deform under excessive loads, absorbing stress and thereby reducing the force transmitted to the tissue. Deployment and grasping are actuated simultaneously via a cable-driven mechanism (Section 2.4), which both folds the device and activates its gripping function (Figure 2C).

2.1 | Design of the Compliant Joints

The foldable structure of OriGrasp relies on compliant joints, which replace screws with elastic deformation to store strain energy like bending springs. Their performance depends on material flexibility and geometry, with approaches such as the membrane technique [33], where thin membranes connect panels as hinges to prevent yielding or failure. According to beam theory, the bending stress (σ) in a thin elastic beam is proportional to the applied moment M

$$\sigma = Mc/I \tag{1}$$

where c is the distance from the neutral axis to the outer fiber of the beam. In rectangular cross-sections $c = t/2$, where t is the thickness of the beam. I is the second moment of area of the beam. Following the Euler–Bernoulli equation, the curvature (κ) relates to the moment and elasticity of the beam as

$$k = M/EI \tag{2}$$

where E is the elastic modulus of the flexible material considered. Combining Equations (1) and (2) and knowing that the curvature κ is inversely proportional to the radius of curvature R, it is possible to obtain that R which prevents yielding, as follows

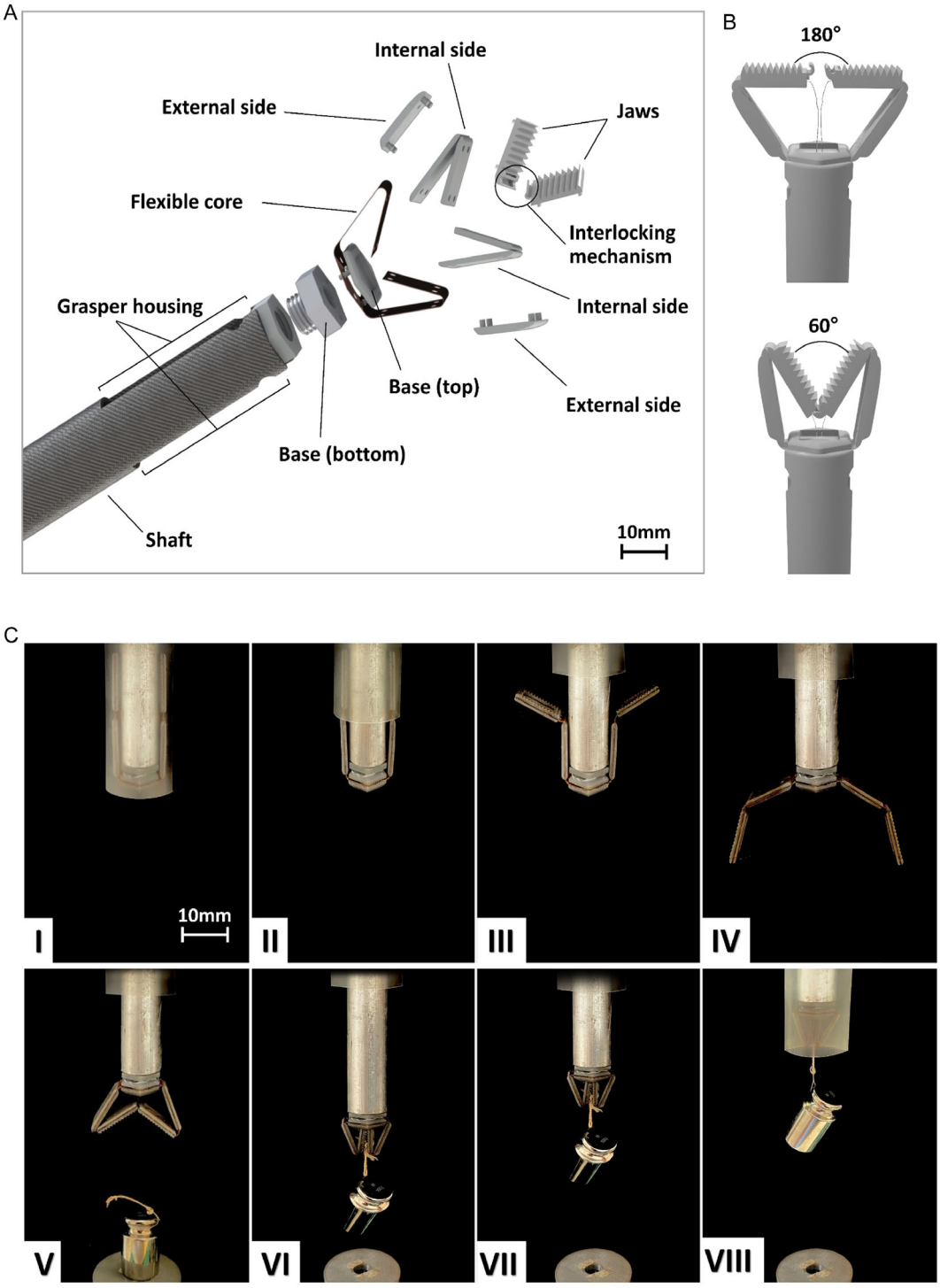

FIGURE 2 | Exploded view of OriGrasp illustrating its components (A). The adjustable opening angle is shown in B. The sequential frames in C (I–VIII) show the deployment process: the device is inserted through the trocar in an unfolded state, reconfigures into grasper mode, grasps a 50 g weight and retracts back inside the trocar.

$$R \geq \frac{Et}{2S_y} \tag{3}$$

where S_y is the yield strength of the material. Similarly to Ynchausti et al. [34], a circular contact was created on the valley side of each fold panel to control the curvature of the membrane, thus controlling the stress distribution. From the derived value of R, it is possible to compute the length of the flexure hinge and the distance Δx between the panels, as shown in Figure 3. These parameters are intended to guide the joint design, minimizing parasitic motion found in other membrane joint types and maintaining membrane stress within allowable limits [35]. Considering the chosen flexible material and an angle of $\theta = 180^{\circ}$ to achieve flat foldability, defined by Butler et al. [36] as the capability of panels to fold compactly and lie parallel, facilitating stowage, transport, and later deployment, the corresponding joint dimensions are presented in Table 2.

TABLE 1 | Design specifications for the development of OriGrasp.

	Description	Value	Units	Reference
Dimensions				
Diameter	Diameter of the instrument	10	mm	[25]
Jaws length	Length of the jaws of conventional graspers	10	mm	[26]
Jaws angle	Angle between the jaws when the grasper is opened	≥60	deg	[31]
Forces				
Pinch force	Pinch force necessary to prevent slip	3.3	N	[28]
Pressure on tissue	Pressure threshold to avoid damage to bowel tissue	329	kPa	[29]
Pulling force	Range of forces required to pull bowel tissue	0.18–1.09	N	[32]
Lifting force	Range of forces required to lift the tissue	0.59–1.21	N	[32]
Output ratio	Ratio between pinch force and actuation force	0.4	—	[30]

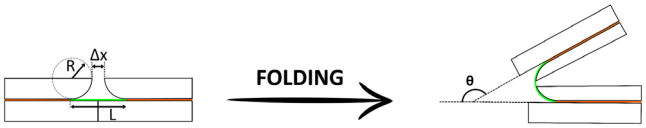

FIGURE 3 | Illustration of the compliant joint based on the membrane technique. Rigid parts, shown in white, are bonded to a flexible sheet. The sheet is shown in red where attached to the rigid parts, and in green where it forms the compliant joint. Circular contacts on the valley side and the parameters used in the model are showed.

2.2 | Modeling of the Compliant Grasper

To guide the design of OriGrasp and define the geometry satisfying the desired specifications, a PRBM of the mechanism was developed. This model supports the definition of geometric parameters according to the target pinch force (4 N) and the output ratio (0.4) of the grasper. The analysis is based on static equilibrium and focuses on the moment balance of the mechanism, with all moments evaluated about the base joint. The joint at the tip was considered kinematically constrained only in the configuration where the jaws are parallel, as the internal rigid components (labeled 1 and 2 in Figure 4) come into contact and acts as hard stop. Outside this configuration, the distal joint is not constrained. The primary external forces are the actuation force F, applied at a horizontal distance d from the base joint, and the reaction force N, opposing the pinch force. The force N is assumed to act normally on the link l_2, which is aligned with the contact surface as the jaws are designed to close almost parallel. Due to the distributed nature of the contact, the equivalent point force is modeled as acting at the midpoint of the link, at a vertical distance $h/2$ from the joint. The restoring torque M, generated by the compliant base joint, is also included. The compliant joint is modeled using the small-length flexural pivot PRBM variant, which is suitable for flexures significantly shorter than the adjacent rigid members [37, 38]. In this model, the flexure is idealized as a pin joint with an equivalent torsional spring. The torsional stiffness K is defined by the elastic and geometric properties of the flexural segment

$$K = \frac{EI}{L} \tag{4}$$

where E is the Young's modulus of the material, I is the second moment of area, and L is the length of the flexure.

Given the width w and thickness t of the cross section, the second moment of area I is given by

$$I = \frac{wt^3}{12} \tag{5}$$

Substituting Equation (5) into Equation (4) yields

$$K = \frac{Ewt^3}{12L} \tag{6}$$

The torque M produced by the joint due to a rotation angle θ is

$$M = K\theta \tag{7}$$

Applying moment equilibrium about the base joint, the following equation is obtained

$$F \cdot d - N \cdot h/2 - K \cdot \theta = 0 \tag{8}$$

where d is assumed to be half of the diameter of the base;

TABLE 2 | Geometric parameters for designing the joints.

Parameter	Description	Formula	Value
Radius of curvature (R)	Minimum radius to prevent yielding of the flexible material	$R \geq \frac{Et}{2S_y}$	1.4 mm
Gap between panels (Δx)	Distance between rigid parts to enable flat foldability and avoid collisions	$\Delta x = R(\pi - 2)$	1.6 mm
Length of the flexure hinge (L)	Length of the flexible part not attached to rigid parts (depicted as a green line in Figure 3)	$L = 2R\left(\frac{\theta}{2} + \cos\left(\frac{\theta}{2}\right)\right)$	4.4 mm

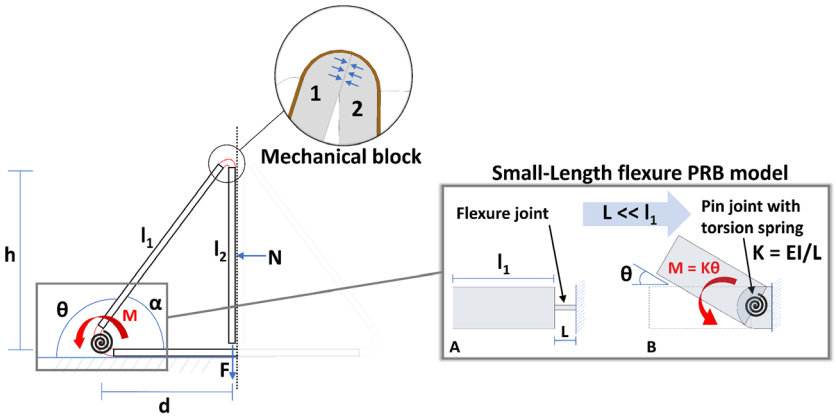

FIGURE 4 | Geometrical representation of the grasper (left), with a detail on the mechanical block created by the contact between rigid components 1 and 2. In this configuration, the contact between 1 and 2 kinematically constrains the tip joint. The equilibrium of moments was evaluated with respect to the joint at the base, which was modeled using the small-length flexure PRB model (right): (A) short-length flexure representation and (B) pseudo-rigid body model (PRBM).

By solving Equation (8) for the actuation force F, we obtain

$$F = \frac{N \cdot h}{2 \cdot d} + \frac{K \cdot \theta}{d} \tag{9}$$

The equation correlates the actuation force F with N and the geometry of the grasper. Specifically, as θ changes, the geometry of the mechanism varies accordingly, affecting the effective lengths and leverage of links l_1 and l_2. Considering a static condition with $N = 4$N, verified when the grasper exerts the required pinch force of 4N, and a distance $d = 5$ mm between the point of application of the actuation force and the center of the compliant joint, the actuation force needed to maintain this condition can be predicted as a function of θ. From this angle, the dimensions of members l_1 and l_2 can be derived through trigonometry, thereby providing the basis for the proper geometric design of the grasper. The model was validated by fabricating a grasper with the derived geometry and performing a pinch test, measuring actuation and pinch forces and comparing them with model predictions. In particular, the rotation angle α (complementary to the angle θ) shown in the geometrical representation of the grasper in Figure 4, was measured experimentally and compared with the model prediction. Although the analytical model provides a useful and straightforward description of the mechanism's behavior, certain discrepancies with experimental results were expected due to the PRBM approximations, tolerances, friction, material variability, and nonlinear flexural effects at large angles. Analyzing these deviations will support design refinement and improve predictive accuracy in future stages.

2.3 | Fabrication and Materials

OriGrasp is fabricated using a layer-by-layer technique, combining 3D printed rigid parts bonded onto a flexible layer with adhesive and mechanically connected using a peg-and-hole system. The flexible material was Kapton (DuPont, USA), chosen for its durability and foldability [39]. The rigid components are fabricated from Biomed Clear, a biocompatible resin by Formlabs (Formlabs Inc, USA), and printed using a Form 3+ SLA 3D printer (Formlabs Inc, USA). The jaws were printed using two 3D printing technologies: the same Form 3+ SLA printer used for the other rigid components of the grasper, and Stratasys J35 Pro (Stratasys Inc., USA), a PolyJet multimaterial printer which allows tunable mechanical properties by mixing rigid (VeroUltraWhite, RGD824) and flexible (ElasticoClear, FLX93) photopolymers. The resulting materials printed with the polyjet multimaterial printer were designated VE_{50} and VE_{85}, with the subscripts indicating their respective Shore hardness values. The details of the fabrication steps, the overall test setup and procedure for the characterization of VE_{50} and VE_{85} and the resulting stress–strain curves are described in Sections S1 and S2 of Supporting Information.

2.4 | Actuation

OriGrasp is actuated by a cable-driven mechanism compatible with both laparoscopic and robotic platforms. It was integrated into a modified Intuitive Surgical EndoWrist, comprising three main components: the housing with four actuated pulleys, the shaft, and the OriGrasp end-effector (substituting the traditional da Vinci grasper). Stainless steel cables with a diameter of 0.25 mm were used to replace the Da Vinci cables and were attached to the jaws, passing through the base channel and the shaft and connected to a pulley inside the housing linked to disk 3, actuated by a servo motor that mirrors the surgeon's console movements. For performance assessment, OriGrasp was driven by an HS-225MG servomotor (Hitec RCD, USA), selected for its compact size, low weight, high speed, and suitable torque (max 470 N·mm) (Figure 5).

3 | Analysis of Jaws-Tissue Interaction

To investigate the interaction between the grasper and soft tissues, various jaw configurations were analyzed using the FEM approach and through experimental pulling tests to identify the best jaw design that captures the trade-off between safe tissue interaction and effective grasping while pulling the tissue.

3.1 | Pressure Distribution

The FEM model provided a computational framework for evaluating the influence of jaw design parameters, such as tooth

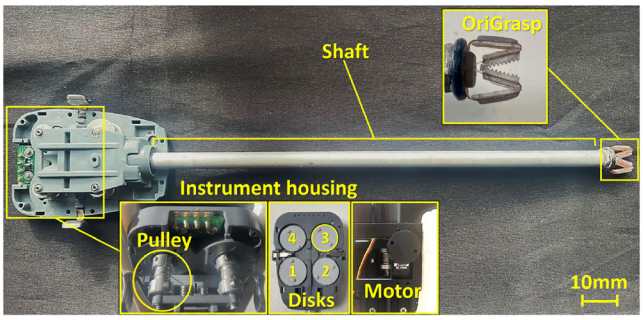

FIGURE 5 | Actuation system: OriGrasp was integrated on an Intuitive Surgical EndoWrist Instrument. The grasper is fixed on the tip of the shaft; the actuation cables are connected to the jaws of the grasper, run through the shaft, and are linked to the pulley of the disk 3, which is actuated by a servo motor.

number and material stiffness, on the pressure distribution resulting from the compression applied to the soft tissue. In laparoscopic instruments, jaw profiles are often engineered to enhance tissue retention while minimizing slippage, as reported by Brown et al. [40]. Based on this evidence, the present study investigates several rounded-tooth jaw configurations, which, as shown in Brown et al., have been demonstrated to reduce tissue damage compared to sharp-toothed designs, albeit at the cost of some reduction in pinch strength. At the same time, the study also explored a simplified design for the jaws, with optimized dimensions and number of teeth, enabling low-cost, reproducible manufacturing, consistent with the overall device strategy.

Three jaw geometries with 4, 8, and 10 teeth were developed by varying the angle and the pitch of the rounded teeth (Figure 6), and keeping tooth height constant.

Using a parametric computer-aided design model,the jaw geometries were imported into ANSYS Workbench (Release 2024R2), which was used to allow flexible design iterations. Soft tissue was modeled as a homogeneous silicone phantom (Ecoflex 00-50, Smooth-On, USA), commonly employed to simulate bowel tissue such as the colon [41]. All jaw materials were defined as linear elastic, with mechanical properties reported in Section S2 of Supporting Information. Boundary conditions replicated the experimental setup and a compressive load of 4N (corresponding to the targeted pinch force of OriGrasp) was applied. Mesh refinement was introduced in regions with high stress gradients and at contact interfaces to ensure accuracy and convergence. The FEM was validated with 8-tooth jaws (Figure 7A) using a Tekscan 5027 Pressure Mapping Sensor (Tekscan Inc., Boston, MA, USA) (S3, Supporting Information), showing strong agreement with experiments. Peak pressures were predicted with a mean error of ≈3% (Figure 7B), while average pressures (Figure 7C) showed slight discrepancies, overestimated for VE_{50A} and underestimated for other materials, with mean errors below 7%, confirming an overall good prediction. The analysis of the pressures revealed clear trends across materials and geometries. VE_{85A} exhibited the highest average pressures, reaching 99 kPa with the 4-tooth profile, while Biomed Clear maintained intermediate pressures (77–88 kPa) and VE_{50A} consistently yielded the lowest pressures (61 kPa with 10 teeth). Peak pressures remained below the safety threshold of 329 kPa for all configurations. Differently from the other materials, jaws made of Biomed Clear reached maximum average and peak pressure (88–265 kPa) with the 8-teeth profile rather than with the 4-teeth design. This difference stems from the material's high stiffness and limited compliance. With only 4 teeth, the rigid Biomed Clear jaw had fewer contact points and less adaptability, which limits effective force transmission and results in lower pressure. Additionally, fewer interlocking elements can compromise lateral stability under tangential loads, raising the risk of slippage in dynamic operations. Increasing the number of teeth to 8 improves pressure distribution and contact efficiency while maximizing peak pressure through a balance between the number and size of the contact points. Conversely, the 10-tooth profile exhibited lower pressure values and less effective grip, suggesting that overly fine and numerous teeth fail to transmit adequate force, particularly in softer materials. In contrast, VE_{85A} and VE_{50A} exhibited the highest peak pressure, employing the 4-tooth profile, with the VE_{85A} reaching 257 kPa and VE_{50A} substantially lower and with a maximum value of 205 kPa. This result aligns with their higher compliance, which allows them to better conform to external loads and distribute pressure more evenly across contact surfaces.

However, the 4-tooth profile concentrates forces on fewer points, increasing the risk of tissue damage and reducing lateral stability. Conversely, the 10-tooth profile, while spreading contact, results in smaller teeth and insufficient grip, especially in softer materials. Based on these considerations, the 8-tooth profile was selected as an optimal compromise in terms of peak and average pressure. Consequently, additional experiments were conducted to measure the pulling force of the grasper using the 8-tooth jaws, each employing a different material.

3.2 | Pulling Force

The 8-tooth jaws were fabricated using Biomed Clear, VE_{50A} and VE_{85A}, and integrated into OriGrasp in order to evaluate how jaw's material affects grasper performance in pulling soft tissues (Figure 7D). Details of the experimental setup are included in the Supplementary Information (S4).

The results (Figure 7E) demonstrate that Biomed Clear showed the best balance, sustaining >0.8 N and retracting tissue up to 29 mm before detachment. VE_{85A} exhibited similar peak force (≈0.8 N) but allowed shorter retraction (≈25 mm). VE_{50A}, while

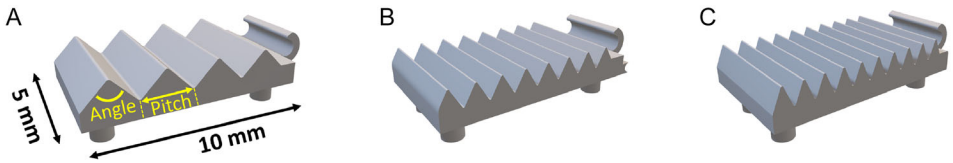

FIGURE 6 | Jaw configurations, all with the same overall size (10 mm long and 5 mm wide), but differing in tooth number and geometry: (A) 4 teeth, pitch 2 mm, angle 90 deg; (B) 8 teeth, pitch 1 mm, angle 60 deg; and (C) 10 teeth, pitch 0.8 mm, angle 45 deg.

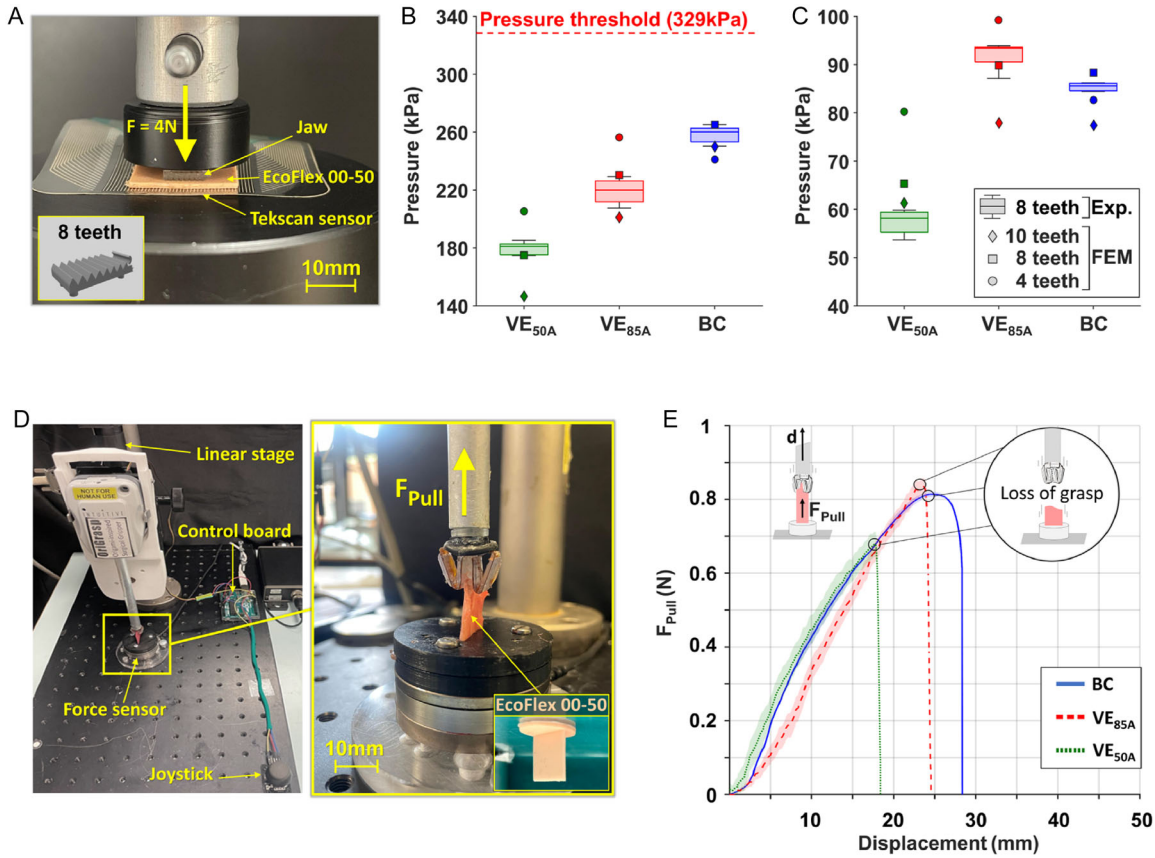

FIGURE 7 | Evaluations of jaws–tissue interaction. Setup of the validation test with details of the 8-tooth jaw's profile used (A). The measured peaks of pressure (B) and average pressures (C) obtained by the experimental test and FEM's predictions. Setup of the pulling test (D) and results obtained using 8-tooth jaws made by Biomed Clear (BC), VE_{50A} and VE_{85A}.

safest in terms of pressure distribution, proved inadequate grasping, failing to sustain 0.7 N and losing grip before 20 mm retraction.

Furthermore, the biocompatibility of Biomed Clear, combined with its use in the other rigid components of the device, made it the most suitable choice to achieve the simplified OriGrasp design. Thus, the Biomed Clear 8-tooth jaws have been selected for the final integration in OriGrasp.

4 | Perfomance of OriGrasp

4.1 | Pinch Force and Mechanical Transmission Efficiency

OriGrasp with the 8-tooth Biomed Clear configuration was tested for pinch force (defined as the force applied on tissue during jaws compression) and for mechanical efficiency, calculated as the ratio of pinch force to actuation force. The pinch force F_{pinch} was

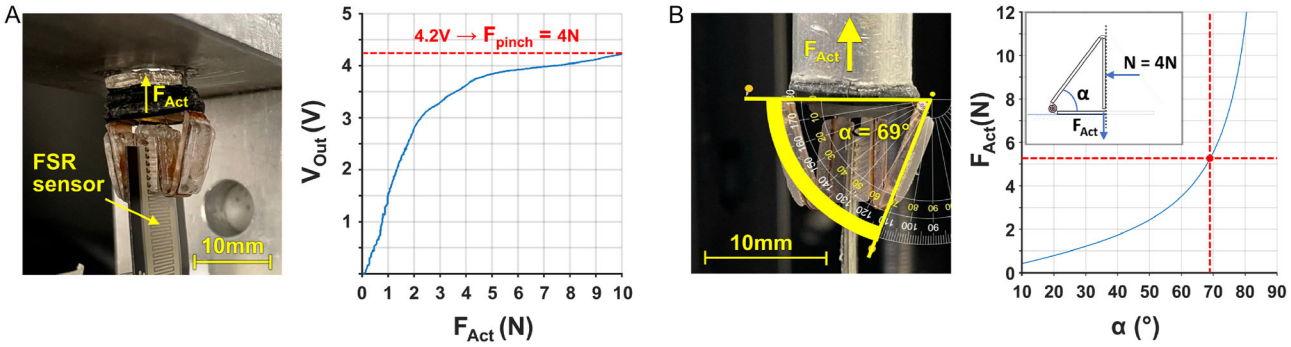

FIGURE 8 | Results of the pinch test (A): on the left, the experimental setup is shown, with the grasper mounted under the testing machine and the FSR sensor positioned between the jaws. On the right, the measured voltage output recorded by the sensor is plotted against the corresponding actuation force (F_{4N}). The measured was obtained by converting the sensor voltage output (4.2 V) into the corresponding force (4 N) through the calibration curve of the sensor, provided in the Supporting Information. In B, the left image shows the grasper when $F_{pinch} = 4$ N with $F_{Act} = 10$ N. The corresponding joint angle was, in agreement with the model predictions. The model output, shown on the right, indicates that for the same angle α, $F_{Act} = 10.5$ N (5.25 N per half grasper) is required to achieve the target F_{pinch} of = 4 N.

recorded using a force-sensing resistor (FSR 408) sensor (Interlink Electronics, Inc., USA), positioned between the jaws, which had been previously calibrated (S5, Supporting Information). The actuation force F_{Act} was evaluated with a Universal Testing Machine (Instron 4464, USA). The grasper was able to exert a pinch force of 4N (Figure 8A) with an actuation force of 10 N, matching the targeted mechanical transmission ratio of 0.4, specified in Table 1. Furthermore, the measured pinch force exceeds the minimum threshold required to prevent tissue slippage, ≈3.3 N [28], suggesting a stable grasp during surgical maneuvers. During grasping, deformation of the compliant joints absorbed part of the actuation force, causing progressive structural collapse and limiting the maximum achievable pinch force. Pulling and lifting tests with motor's inputs above 10 N confirmed this limitation, as the pinch force remained capped at about 4 N. This self-limiting response enables the grasper to act as a mechanical fuse for gentle interaction with delicate tissues. The grasper was fabricated according to the parameters derived from the static model, aiming for $F_{pinch} = 4$ N at 40% efficiency. The experimental tests confirmed the model's predictions. As shown in Figure 8B, for $\alpha = 69$ deg the model estimates $F_{Act} = 5.25$ N per half grasper, corresponding to a total force of 10.5 N. Experimentally, the required $F_{Act} = 10$ N represents a discrepancy of only about 5% compared to the model. Such consistency validates the accuracy of the model and supports its applicability for further optimization.

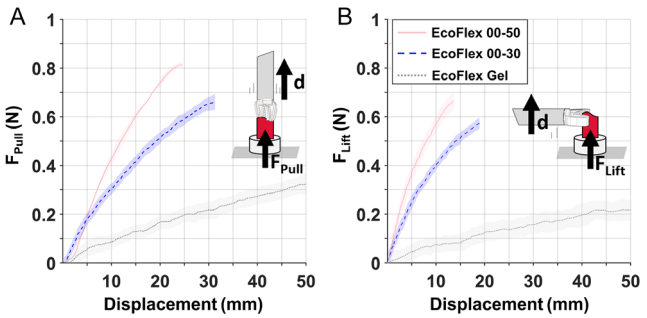

FIGURE 9 | (A) Pulling and (B) lifting forces of the grasper manipulating silicone tissues with different stiffness. The three silicone tissues fabricated with different hardness levels, simulate three different stiffnesses of the intestinal tissue.

4.2 | Pulling and Lifting Force

The grasper's performance was then assessed through pulling and lifting tests on three silicone specimens of varying stiffness (EcoFlex 00-50, 00-30, and Gel), commonly used in literature for simulating different regions of bowel tissue, such as colon [41], rectum [42] and adipose tissue [43]. A sample of ex vivo porcine

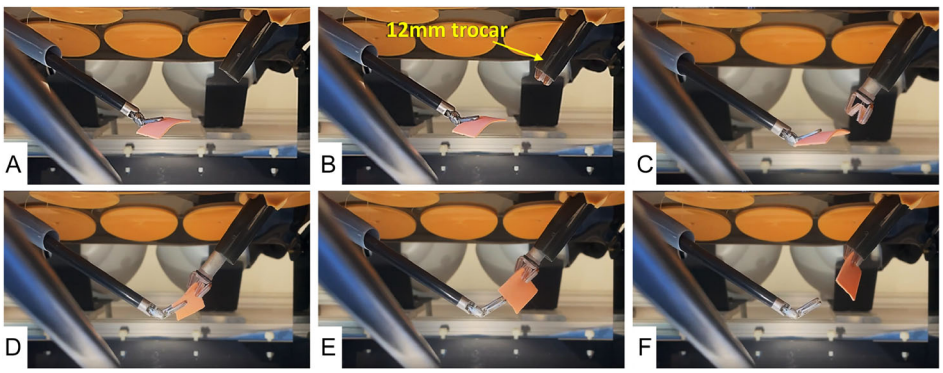

FIGURE 10 | Grasping and retraction of a silicone-made sample inside a simulated abdominal cavity: (A) the 8 mm da Vinci grasper grasps the sample; (B) OriGrasp is deployed through a 12 mm trocar; (C) the da Vinci grasper orients the sample toward OriGrasp, which begins to approach it; (D) OriGrasp grasps the sample; (E) OriGrasp begins the retraction while the da Vinci grasper releases its grip; and (F) OriGrasp fully retracts the sample into the trocar.

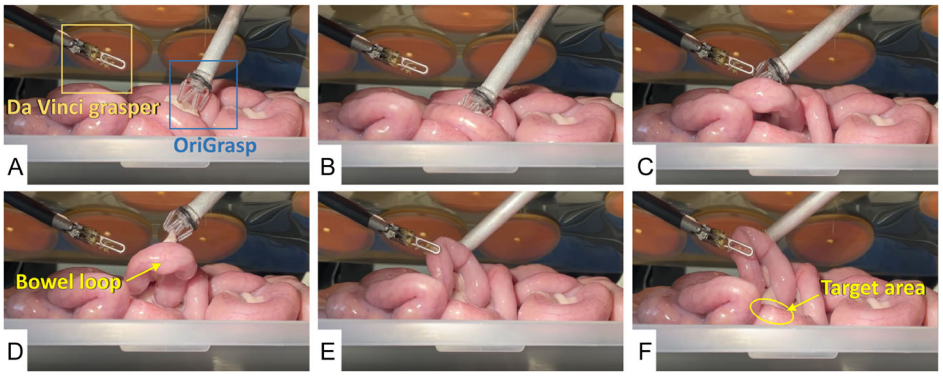

FIGURE 11 | Sequence of OriGrasp manipulating porcine bowel tissue: (A) OriGrasp approaches the tissue; (B) grasps it securely; (C) repositions the tissue; (D) lifts the bowel loop; (E) moves the bowel loop behind the 8 mm da Vinci grasper; and (F) clears the target area by removing the loop from its original location, allowing access for the da Vinci grasper.

TABLE 3 | Comparison between OriGrasp and atraumatic surgical graspers reported in the literature. Devices are compared in terms of surgical task, minimum trocar diameter, structure indicating how the device is built in terms of material properties (rigid, soft, or a rigid-soft hybrid), multifunctionality, design complexity (qualitatively scored from low = • ∘∘∘∘ to high = •••••, including actuation system to account for manufacturing, assembly and maintenance), robotic platform used for the integration and key features.

Reference	Task	Trocar	Structure	Multi-function	Design complexity	Robot integration	Key features
Kinnicutt et al. [8]	Safe retraction intestines	≥18 mm	Hybrid	Yes	•••• ∘	Ue5 Universal robot arm	Soft actuator-based, safe retraction, detachable functionality.
Guo et al. [45]	Delicate nerve manipulation	≥5 mm	Soft	No	••• ∘∘	Not tested	Soft actuator-based, low grasping force (1 N).
Klok et al. [46]	Atraumatic grasping laparoscopy	≥5 mm	Rigid	No	• ∘∘∘∘	Not tested	Compliant, monolithic structure, 43% efficiency.
Guo et al. [47]	Delicate surgical manipulation	≥9 mm	Hybrid	No	••• ∘∘	Not tested	Embedded soft actuators, multi-contact gripping; rigid hook shell.
O'Hanley et al. [48]	Internal organ manipulation	≥12 mm	Soft	No	•••• ∘	Not tested	Three-fingered geometric grasp; modular 3D printed design.
Frecker et al. [49]	MIS (lap/ophth)	≥5 mm /0.5 mm	Rigid	Yes	• ∘∘∘∘	Not tested	Monolithic compliant mechanism; 0.3 N grasping force.
Gafford et al. [50]	Tissue manipulation pancreas	≥15 mm	Soft	Yes	•••••	Not tested	Distributes force safely; lifts porcine pancreas 80 g.
Mykhailyshyn et al. [21]	Low-contact MIS	≥26 mm	Rigid	No	•••• ∘	Yaskawa SDA10F robot arm	Lifts up to 3.5 N; low-contact grasping; friction elements mitigate slippage.
Goyzueta et al. [51]	Tissue manipulation laparoscopy	—	Hybrid	No	•• ∘∘∘	Not tested	Compliant monolithic jaws, max pinch 3.5 N, pulling 1.4 ± 0.6 N.
Ju et al. [52]	Tumor palpation/clamping	≥12 mm	Rigid	Yes	•••• ∘	Not tested	Detects tumors; senses clamping status.
Liu et al. [20]	Grasping, retraction, palpation	≥13 mm	Hybrid	Yes	•••••	Tested on dVRK	Three snake-like fingers; integrated force sensors; configurable modes.
Edmondson et al. [16]	General robotic surgery	≥19 mm	Rigid	Yes	•• ∘∘∘	Not tested	Monolithic, origami-inspired; scalable and sterilizable.
Sun et al. [53]	Manipulating sensitive organs	≥12 mm	Soft	No	•• ∘∘∘	Not tested	Monolithic compliant mechanism; delicate adaptive grasping.
Lee et al. [54]	Drug delivery grasper	≥5/10.5 mm	Hybrid	No	••• ∘∘	Not tested	Soft-foldable actuators; max grasp 180 mN.
OriGrasp	Abdominal tissue manipulation	≥12 mm	Hybrid	Yes	• ∘∘∘∘	Tested on dVRK	Reconfigurable origami-inspired design; flexible, easy to manufacture; safe grasp 4 N.

intestinal tissue was also used to provide a reference for the grasper interaction with a real tissue and to allow comparison with the simulated silicone models. The porcine tissue was sourced from a local slaughterhouse (same-day euthanasia). The specimen used for the test was explanted and cleaned by a licensed veterinarian and immediately transported to the laboratory, ensuring minimal deterioration and preservation of the tissue's physiological properties. It was included only in the pulling test, where dynamic interactions, such as friction, adhesion and tissue irregularities, play a significant role and are hard to replicate with synthetic materials. In contrast, the compression test primarily relies on overall stiffness, which can be reliably reproduced using silicone samples. The results obtained with the ex vivo tissue (S6, Supporting Information) closely matched those observed with Ecoflex 00-50, confirming the suitability of this material as a reliable synthetic analogue for the experimental evaluations conducted during the jaw design investigation. No additional ex vivo tissue was used for the lifting test, as any relevant similarities between the ex vivo tissue and the simulated silicone models would have already emerged from the pulling test. The results further confirmed the safe and effective operation of the instrument. The instrument matched the requirements, achieving lifting and pulling force values in accordance with benchmarks reported in the current literature for safe handling of intestinal tissues. Specifically, in tests involving Ecoflex 00-50 and Ecoflex 00-30 phantoms, the grasper generated pulling forces of slightly more than 0.6 and 0.8N, and lifting forces of ≈0.6 and 0.7 N (Figure 9). These results align with the range (0.17–1.21 N) indicated by Ranzani et al. [32] as appropriate for the atraumatic yet effective manipulation of intestinal structures. Moreover, the grasper also demonstrated the ability to interact with softer and more delicate tissue surrogates, such as adipose-mimicking materials (Ecoflex Gel), pulling and lifting the material with appropriate forces (0.2 and 0.3 N) and reaching the maximum retraction without inducing macroscopic damage, rupture or tearing. This highlights the grasper's ability to strike a balance between sufficient mechanical engagement and compliance.

4.3 | Integration and Validation on a Surgical Robotic Platform

To evaluate the ease of integration and control of the OriGrasp within a robotic surgical environment, the instrument was adapted to be used on a dVRK platform (Figure S9).

The dVRK architecture, composed of both master tool manipulators and patient side manipulators, has already been presented in the literature [44]. All details regarding the system overview are provided in Section S7, Supporting Information. The successful integration and use of OriGrasp with the dVRK was confirmed through two feasibility demonstrations. The first demonstration assessed the device's controllability within a simulated abdominal cavity (Figure 10). OriGrasp was introduced through a 12 mm trocar, used to grasp a soft tissue phantom with the left robotic instrument and retracted back through the same trocar, demonstrating effective insertion, manipulation, and withdrawal capabilities.

The second demonstration focused on the manipulation of ex vivo porcine bowel tissue (Figure 11). The tissue used in this demo was a porcine intestinal segment obtained and prepared following the same procedure used in Section 4.2. To preserve its physiological properties, the demo was performed immediately upon the tissue's arrival in the laboratory. The operator guided OriGrasp toward a bowel loop, successfully grasped and elevated the tissue, thereby exposing the underlying surgical field. This maneuver enabled clear access for a secondary instrument (8 mm da Vinci grasper) mounted on the opposing dVRK arm, simulating a clinically relevant bimanual interaction.

4.4 | Comparative Analysis with the State of the Art

Compared to existing atraumatic graspers reported in literature (Table 3), OriGrasp combines tailored pinch force, a deformable structure that limits excessive tissue pressure, a low-complexity design for reproducible manufacturing and an origami-inspired architecture that enables deployability and multifunctionality within a compact form factor. Unlike fully rigid instruments equipped with force sensors, such as [20], which may offer safe grasping but lack intrinsic compliance, OriGrasp ensures tissue safety through its deformable structure, which was demonstrated to limit excessive pressure during grasping. Similarly, in contrast to soft actuator-based tools [8], [45], and [47] or vortex-based grippers [21], OriGrasp does not rely on bulky external components and does not require large access ports, thereby enhancing its compatibility with most common MIS setups. When compared to other multifunctional designs, such as those proposed in [20, 49, 52], OriGrasp stands out for its origami-inspired architecture, which enables deployability, reconfigurability, and dual functionality while maintaining a low-complexity, easy-to-fabricate design and easy to integrate with commercial surgical robotic platforms (da Vinci robotic system). Finally, unlike other origami-inspired instruments, such as the device proposed in [16], OriGrasp was specifically designed to be inserted safely in its compact, unfolded configuration within the trocar, without exposing any sharp or protruding elements that could damage surrounding tissues. Moreover, it was specifically tested and validated in surgical robotic scenarios, demonstrating its effectiveness in delicate abdominal procedures and underscoring its potential for clinical adoption. The combination of all these features, tissue safety, mechanical efficiency, and manufacturing simplicity, positions OriGrasp as a scalable and practical alternative to current instruments, contributing to the development of accessible, atraumatic robot-integrated surgical tools.

5 | Conclusion

MIS continues to face challenges in designing instruments which are both safe and effective in manipulating delicate soft tissues, particularly in abdominal procedures, while remaining easy to manufacture and maintain. Traditional rigid instruments, while precise, often lack the compliance needed to handle anatomical structures such as the bowel without risk of trauma. Although advanced surgical platforms have emerged, the availability of compliant and cost-effective instruments remains a bottleneck limiting their widespread adoption and versatility. In this context, the experimental validation of OriGrasp confirms its potential as a novel, effective, and safe solution for abdominal tissue manipulation, addressing limitations observed in the literature. Unlike existing origami-inspired surgical instruments

focused mainly on miniaturization or structural simplification, OriGrasp is explicitly engineered for a specific clinical application and validated for bowel handling, where compliance and safety are essential. Regarding its mechanical performance, the grasper generated a pinch force of ≈4 N, sufficient to securely grasp intestinal tissue while remaining well below the threshold for damage. Notably, OriGrasp achieves safe and effective grasping without embedded sensors or complex feedback systems, relying instead on its intrinsically deformable structure to limit excessive forces and maintain a lightweight design.

During pulling and lifting tests, on synthetic phantoms and on ex vivo porcine intestine, it achieved force values comparable to commercial graspers despite its miniaturized and compliant nature.

The integration of OriGrasp into a surgical robotic platform was demonstrated through its implementation on the da Vinci surgical system. Its cable-driven actuation mechanism allows straightforward integration with existing robotic interfaces, ensuring seamless translation into clinical workflows without major modifications to the surgical setup.

Additionally, the foldable structure enables dual functionality: it can act first as an introducer for diagnostic or therapeutic tools and then be deployed as a compliant grasper. This reconfigurability allows to reduce tool exchanges during surgery, thereby streamlining procedural workflows. Future research will aim to further explore and validate this reconfigurability potential, which has been conceptually introduced in this study. In particular, efforts will focus on showing the introducer functionality of OriGrasp by integrating interchangeable end-effectors. Potential applications include coupling the device with suction irrigation units to support intraoperative cleaning and fluid management, or with miniaturized tactile probes to enable tissue palpation and characterization.

In conclusion, OriGrasp introduces an origami-guided approach to the design of robotic MIS tools for abdominal surgery, transforming foldable structures into compact, compliant, and multifunctional instruments. By harnessing foldability not only for miniaturization but also for intrinsic safety and versatility, OriGrasp lays the foundation for a new class of smarter, safer, and more accessible surgical instruments, tailored to diverse procedures, anatomies and robotic platforms.

Author Contributions

Lorenzo Mocellin: conceptualization (lead), data curation (lead), investigation (lead), methodology (lead), project administration (lead), validation (lead), visualization (lead), writing – original draft (lead). **Niccoló Pagliarani:** data curation (supporting), visualization (supporting), writing original draft (supporting), writing – review & editing (equal). **Giulia Gamberini:** resources (supporting), writing – review & editing (equal). **Gastone Ciuti:** supervision (equal), writing – review & editing (supporting). **Matteo Cianchetti:** supervision (equal), writing – review & editing (supporting). **Arianna Menciassi:** supervision (lead), writing – review & editing (supporting).

Acknowledgements

The authors acknowledge the support of the European Union by the Next Generation EU project ECS00000017 'Ecosistema dell'Innovazione' Tuscany Health Ecosystem (THE, PNRR, Spoke 9: Robotics and Automation for Health) and BRIEF - Biorobotics Research and Innovation Engineering Facilities.

Open access publishing facilitated by Scuola Superiore Sant'Anna, as part of the Wiley - CRUI-CARE agreement.

Funding

This work was supported by European Union – Next Generation EU (IR0000036, ECS00000017).

Conflicts of Interest

The authors declare no conflicts of interest.

Data Availability Statement

The data that support the findings of this study are available from the corresponding author upon reasonable request.

References

1. R. Barua, and S. Bhowmik, "Advances of the Robotics Technology in Modern Minimally Invasive Surgery," *Design and Control Advances in Robotics*, no. 1 (2023): 91–104.

2. O. M. Omisore, S. Han, J. Xiong, H. Li, Z. Li, L. Wang, and O. M. Omisore, "A Review on Flexible Robotic Systems for Minimally Invasive Surgery," *IEEE Transactions on Systems, Man, and Cybernetics: Systems* 52, no. 1 (2020): 631–644.

3. B. Johansson, E. Eriksson, B. Berglund, and I. Lindgren, "Robotic Surgery: Review on Minimally Invasive Techniques, Fusion of Multidisciplinary Research," *An International Journal* 2, no. 2 (2021): 201–210.

4. K. Chandrasekaran and A. Thondiyath, "Design of a Tether-Driven Minimally Invasive Robotic Surgical Tool with Decoupled Degree-of-Freedom Wrist," *The International Journal of Medical Robotics and Computer Assisted Surgery* 16, no. 3 (2020): e2084.

5. D. Rus and M. T. Tolley, "Design, Fabrication and Control of Origami Robots," *Nature Reviews Materials* 3, no. 6 (2018): 101–112.

6. J. Wu, X. Guo, X. Pan, J. Hua, Y. Cen, and S. Li, "Origami-Kirigami Structures and Its Applications in Biomedical Devices," *Biomedical Materials & Devices* 3, no. 1 (2024): 1–17.

7. T. Yisi, J. Jiang, J. Huang, J. Sui, and S. Yang, "A Review of Wrist Mechanism Design and the Application in Gastrointestinal Minimally Invasive Surgery of Multi-Degree-of-Freedom Surgical Laparoscopic Instruments," *Surgical Endoscopy* 39, no. 1 (2024): 1–23.

8. L. Kinnicutt, L. T. Gaeta, J. Rogatinsky, J. Lee, A. Cameron, and A. J. Naik, "A Soft Robotic, Modular Laparoscopic Grasper for Atraumatic Retraction of the Small Intestine," *Device* 2, no. 10 (2024), 100560.

9. S. De, J. Rosen, A. Dagan, B. Hannaford, P. Swanson, and M. Sinanan, "Assessment of Tissue Damage due to Mechanical Stresses," *The International Journal of Robotics Research* 26, no. 11-12 (2007): 1159–1171.

10. A. J. Hayanga, K. Bass-Wilkins, and G. B. Bulkley, "Current Management of Small-bowel Obstruction," *Advances in Surgery* 39 (2005): 1–33.

11. M. van der Voort, E. A. M. Heijnsdijk, and D. J. Gouma, "Bowel Injury as a Complication of Laparoscopy," *Journal of British Surgery* 91, no. 10 (2004): 1253–1258.

12. E. P. Westebring-van der Putten, J. J. van den Dobbelsteen, R. H. M. Goossens, J. J. Jakimowicz, and J. Dankelman, "Force Feedback Requirements for Efficient Laparoscopic Grasp Control," *Ergonomics* 52, no. 9 (2009): 1055–1066.

13. C. Brochhausen, V. H. Schmitt, C. N. E. Planck, T. K. Rajab, D. Hollemann, and C. Tap-prich, "Current Strategies and Future

Perspectives for Intraperitoneal Adhesion Prevention," *Journal of Gastrointestinal Surgery* 16, no. 6 (2012): 1256–1274.

14. M. Marco, J. Cai, Q. Zhang, et al., "Engineering Origami: A Comprehensive Review of Recent Applications, Design Methods, and Tools," *Advanced Science* 8, no. 13 (2021): 2000636.

15. L. M. Fonseca, G. V. Rodrigues, and M. A. Savi, "An Overview of the Mechanical Description of Origami-inspired Systems and Structures," *International Journal of Mechanical Sciences* 223 (2022): 107316.

16. B. J. Edmondson, L. A. Bowen, C. L. Grames, S. P. Magleby, and L. L. Howell T. C. Bateman, "Oriceps: Origami-inspired Forceps," *Smart Materials, Adaptive Structures and Intelligent Systems* 56031 (2013): V001T01A027.

17. M. Salerno, K. Zhang, A. Menciassi, and J. S. Dai, "A Novel 4-DOF Origami Grasper with an SMA-Actuation System for Minimally Invasive Surgery," *IEEE Transactions on Robotics* 32, no. 3 (2016): 484–498.

18. H. Suzuki and R. J. Wood, "Origami-inspired Miniature Manipulator for Teleoperated Microsurgery," *Nature Machine Intelligence* 2, no. 8 (2020): 437–446.

19. M. Boyvat, J.-S. Koh, and R. J. Wood, "Addressable Wireless Actuation for Multijoint Folding Robots and Devices," *Science Robotics* 2, no. 8 (2017): eaan1544.

20. H. Liu, M. Selvaggio, P. Ferrentino, et al., "The MUSHA Hand II: A Multifunctional Hand for Robot-Assisted Laparoscopic Surgery," *IEEE/ASME Transactions on Mechatronics* 26, no. 1 (2020): 393–404.

21. R. Mykhailyshyn, and A. M. Fey, "Low-Contact Grasping of Soft Tissue Using a Novel Vortex Gripper," in *International Symposium on Medical Robotics (ISMR)* (IEEE, 2024), pp. 1–6.

22. R. J. Lang, T. Nelson, S. Magleby, and L. Howell, "Thick Rigidly Foldable Origami Mechanisms Based on Synchronized Offset Rolling Contact Elements," *Journal of Mechanisms and Robotics* 9, no. 2 (2017): 1642-4302.

23. T. Tachi, "Rigid-Foldable Thick Origami," *Origami* 5, no. 5 (2011): 253–264.

24. L. A. Bowen, C. L. Grames, S. P. Magleby, L. L. Howell, and R. J. Lang, "A Classification of Action Origami as Systems of Spherical Mechanisms," *Journal of Mechanical Design* 135, no. 11 (2013): 111008.

25. S. Uk Bae, W. K. Jeong, and S. K. Baek, "Current Status of Robotic Single-Port Colonic Surgery," *The International Journal of Medical Robotics and Computer Assisted Surgery* 13, no. 1 (2017): e1735.

26. Y. Huan, I. Tamadon, C. Scatena, et al., "Soft Graspers for Safe and Effective Tissue Clutching in Minimally Invasive Surgery," *IEEE Transactions on Biomedical Engineering* 68, no. 1 (2020): 56–67.

27. E. A. M. Heijnsdijk, H. de Visser, and J. Dankelman, "Slip and Damage Properties of Jaws of Laparoscopic Graspers," *Surgical Endoscopy* 18 (2004): 974–979.

28. E. A. M. Heijnsdijk, A. Pasdeloup, J. Dankelman, and D. J. Gouma, "The Optimal Mechanical Efficiency of Laparoscopic Forceps," *Surgical Endoscopy* 18 (2004): 1766–1770.

29. A. F. Khan, M. K. Macdonald, C. Streutker, C. Rowsell, J. Drake, and T. Grantcharov, "Defining the Relationship between Compressive Stress and Tissue Trauma during Laparoscopic Surgery Using Human Large Intestine," *IEEE Journal of Translational Engineering in Health and Medicine* 7 (2019): 1–8.

30. E. M. Olig, S. Wilson, and M. Reddy, "Output Force and Ratio of Laparoscopic Graspers: An Evaluation of Operating Room Ergonomics," *American Journal of Obstetrics and Gynecology* 229, no. 3 (2023): 307–e1.

31. A. Sakes, K. Hovland, G. Smit, J. Geraedts, and P. Breedveld, "Design of a Novel Three-Dimensional-Printed Two Degrees-of-Freedom Steerable Electrosurgical Grasper for Minimally Invasive Surgery," *Journal of Medical Devices* 12, no. 1 (2018): 011007.

32. T. Ranzani, G. Ciuti, G. Tortora, et al., "A Novel Device for Measuring Forces in Endoluminal Procedures," *International Journal of Advanced Robotic Systems* 12, no. 8 (2015): 116.

33. R. J. Lang, K. A. Tolman, E. B. Crampton, S. P. Magleby, and L. L. Howell, "A Review of Thickness-Accommodation Techniques in Origami-Inspired Engineering," *Applied Mechanics Reviews* 70, no. 1 (2018): 010805.

34. C. Ynchausti, S. Shirley, S. P. Magleby, and L. L. Howell, "Adjustable, Radii-controlled Embedded Lamina (RadiCEL) Hinges for Folding of Thick Origami-adapted Systems," *Mechanism and Machine Theory* 187 (2023): 105361.

35. F. Patrick, J. Finder, and C. Hühne, "Test Methods for the Mechanical Characterization of Flexure Hinges," *Experimental Mechanics* 63, no. 7 (2023): 1203–1222.

36. J. Butler, N. Pehrson, and S. Magleby, "Folding of Thick Origami through Regionally Sandwiched Compliant Sheets," *Journal of Mechanisms and Robotics* 12, no. 1 (2020): 011019.

37. L. L. Howell, "Compliant Mechanisms," in *st Century Kinematics: The 2012 NSF Workshop* (Springer, 2013): 189–216.

38. L. L. Howell and A. Midha, "A Method for the Design of Compliant Mechanisms with Small-Length Flexural Pivots," *Journal of Mechanical Design* 116, no. 1 (1994): 280–290.

39. Z. Zhakypov and J. Paik, "Design Methodology for Constructing Multimaterial Origami Robots and Machines," *IEEE Transactions on Robotics* 34, no. 1 (2018): 151–165.

40. A. W. Brown, S. I. Brown, D. Mclean, Z. Wang, and A. Cuschieri, "Impact of Fenestrations and Surface Profiling on the Holding of Tissue by Parallel Occlusion Laparoscopic Graspers," *Surgical Endoscopy* 28 (2014): 1277–1283.

41. M. Finocchiaro, C. Zabban, Y. Huan, et al., "Physical Simulator for Colonoscopy: A Modular Design Approach and Validation," *IEEE Access* 11 (2023): 36945–36960.

42. Z. Mao, S. Suzuki, A. Wiranata, Y. Zheng, and S. Miyagawa, "Bio-inspired Circular Soft Actuators for Simulating Defecation Process of Human Rectum," *Journal of Artificial Organs* 28 no. 2 (2024): 252-261.

43. N. Joshi and T. Roman-Micek, "Technology and Innovation," *Comprehensive Healthcare Simulation: Operations, Technology, and Innovative Practice 1* (2019): 315–338.

44. C. D'Ettorre, A. Mariani, A. Stilli, et al., "Accelerating Surgical Robotics Research: A Review of 10 years with the da Vinci Research Kit," *IEEE Robotics & Automation Magazine* 28, no. 4 (2021): 56–78.

45. J. Guo, J.-H. Low, X. Liang, J. S. Lee, Y.-R. Wong, and R. Chen Hua Yeow, "A Hybrid Soft Robotic Surgical Gripper System for Delicate Nerve Manipulation in Digital Nerve Repair Surgery," *IEEE/ASME Transactions on Mechatronics* 24, no. 4 (2019): 1440–1451, https://doi.org/10.1109/TMECH.2019.2924518.

46. J.-W. Klok, R. Postema, A. T. Steinþorsson, J. Dankelman, and T. Horeman, "Design and Evaluation of a Balanced Compliant Laparoscopic Grasper," *IEEE Journal of Translational Engineering in Health and Medicine* 11 (2023): 451–459.

47. Jin Guo, Yi Sun, Xinquan Liang, et al., "Design and Fabrication of a Pneumatic Soft Robotic Gripper for Delicate Surgical Manipulation," *IEEE International Conference on Mechatronics and Automation* (2017): 1069–1074, https://doi.org/10.1109/ICMA.2017.8016024.

48. H. O'Hanley, M. Rosario, Y. Chen, A. Maertens, J. Walton, and J. Rosen, "Design and Testing of a Three Fingered Flexural Laparoscopic Grasper," *Transactions of the ASME-W-Journal of Medical Devices* 5, no. 2 (2011): 027508.

49. M. I. Frecker, K. M. Powell, and R. Haluck, "Design of a Multifunctional Compliant Instrument for Minimally Invasive Surgery," *Journal of Biomechanical Engineering* 127, no. 6 (2005): 990–993, https://doi.org/10.1115/1.2056560.

50. Joshua Gafford, Ye Ding, Andrew Harris, et al., "Shape Deposition Manufacturing of a Soft, Atraumatic, and Deployable Surgical Grasper," *Journal of Mechanisms and Robotics* 7, no. 2 (2015): 021006.

51. A. Goyzueta, C. Nelson, B. Woodin, and L. Gu, "Experimental Analysis of Jaw-Tissue Interaction Forces Using a Compliant Surgical Grasper," *Journal of Medical Devices* 7, no. 2 (2013): 020917.

52. F. Ju, X. Luo, and L. Ding, "Multifunctional Robotic Surgical Forceps with Tactile Sensor Array for Tissue Palpation and Clamping Status Detection," *IEEE Sensors Journal* 24, no. 10 (2024): 16883–16891.

53. Y. Sun, Y. Liu, L. Xu, Y. Zou, A. Faragasso, and T. C. Lueth, "Automatic Design of Compliant Surgical Forceps with Adaptive Grasping Functions," *IEEE Robotics and Automation Letters* 5, no. 2 (2020): 1095–1102.

54. Hun Chan Lee, Nash Elder, Matthew Leal, et al., "A Fabrication Strategy for Millimeter-Scale, Self-Sensing Soft-Rigid Hybrid Robots," *Nature Communications* 15, no. 1 (2024): 8456, https://doi.org/10.1038/s41467-024-51137-8.

Supporting Information

Supporting Information is available from the Wiley Online Library or from the author. **Supporting Fig. S1:** Illustration of the materials used to fabricate OriGrasp (A) and the manufacturing process (B). **Supporting Fig. S2:** Dimensions of the specimens tested: dogbone's shape for the tensile test (A) and cylindrical shape for the compression test (B). **Supporting Fig. S3:** Results of tensile tests and compression tests for VE_{85} (A,B) and VE_{50} (C,D). **Supporting Fig. S4:** Setup for the pulling test. **Supporting Fig. S5:** Setup for the lifting test. **Supporting Fig. S6:** Setup for the calibration of the FSR sensor. **Supporting Fig. S7:** FSR calibration curve. **Supporting Fig. S8:** Pulling force of the grasper during manipulation of ex vivo porcine bowel tissue. The pulling force curve obtained from the previous test on Ecoflex 00-50 is included for comparison with the ex vivo tissue. **Supporting Fig. S9:** Setup for the integration with dVRK: A) Master Tool Manipulators (MTM1, MTM2); B) Patient Side Manipulators (PSM1, PSM2); C) back view of the instrument housing showing the actuation disk 3 used to actuate the instrument; D) OriGrasp and traditional 8-mm da Vinci grasper. **Supporting Table S1:** Jaw configurations with varying tooth geometry and material. **Supporting Table S2:** Mechanical properties of VE_{50} and VE_{85} and Biomed Clear (BC).